

Immunity of the second harmonic shear horizontal waves to adhesive nonlinearity for breathing crack detection

Fuzhen Wen, Shengbo Shan and Li Cheng

Department of mechanical engineering, The Hong Kong Polytechnic University, Kowloon, Hong Kong.

The Hong Kong Polytechnic University Shenzhen Research Institute, Shenzhen 518057, China.

Hong Kong Branch of National Rail Transit Electrification and Automation Engineering Technology Research Center, The Hong Kong Polytechnic University, Kowloon, Hong Kong.

E-mail: li.cheng@polyu.edu.hk

Abstract

High-order harmonic guided waves are sensitive to micro-scale damage in thin-walled structures, thus conducive to its early detection. In typical autonomous structural health monitoring (SHM) systems activated by surface-bonded piezoelectric wafer transducers, adhesive nonlinearity (AN) is a non-negligible adverse nonlinear source that can overwhelm the damage-induced nonlinear signals and jeopardize the diagnosis if not adequately mitigated. This paper first establishes that the second harmonic shear horizontal (2nd SH) waves are immune to AN while exhibiting strong sensitivity to cracks in a plate. Capitalizing on this feature, the feasibility of using 2nd SH waves for crack detection is investigated. Finite element (FE) simulations are conducted to shed light on the physical mechanism governing the 2nd SH wave generation and their interaction with the contact

acoustic nonlinearity (CAN). Theoretical and numerical results are validated by experiments in which the level of the AN is tactically adjusted. Results show that the commonly used second harmonic S0 (2nd S0) mode Lamb waves are prone to AN variation. By contrast, the 2nd SH0 waves show high robustness to the same degree of AN changes while preserving a reasonable sensitivity to breathing cracks, demonstrating their superiority for SHM applications.

Keywords: Shear horizontal waves, Second harmonics, Adhesive nonlinearity, Contract acoustic nonlinearity, Experimental study

1. Introduction

Materials and engineering structures experience a continuous accumulation of mechanical damage during their service. Among various damage modalities, cracks are common and insidious, especially in metal structures [1,2]. Progressive crack propagation from microscopic to macroscopic stages might rapidly lead to structural failure without timely awareness and remedial actions. To ensure structural safety and avoid catastrophic consequences, effective early detection strategies are vital.

Structural health monitoring (SHM) techniques based on nonlinear guided waves (NGWs) have gained increasing popularity due to their exceptionally high sensitivity to small defects or even microstructural changes in materials [3]. A rich body of NGW-based SHM approaches focuses on damage identification using higher harmonic phenomena [4-8]. Specifically, the one based on the second harmonic waves, predominantly the second harmonic Lamb waves (2nd Lamb waves), has been extensively exploited, i.e., for the

detection of micro-scale defects in weakly nonlinear plates [7,9-20]. For example, experimental studies show that the second harmonic S0 (2nd S0) mode exhibits a much higher sensitivity to breathing cracks than the second harmonic A0 (2nd A0) mode [7,9]. However, the 2nd S0 waves are also vulnerable to other unwanted nonlinear sources in a practical SHM system [21]. In particular, when transducers need to be bonded on the surface of a structure, a crucial nonlinear source stems from the inherent adhesive nonlinearity (AN) of the bonding layer, which is non-negligible and might even overwhelm the damage-related information. Frequency tuning characteristics of the AN-induced 2nd S0 waves were reported by Shan *et al.* [22]. Such information can be used to optimize the system configuration, such as the dimension of the Lead Zirconate Titanate (PZT) wafer transducers and the excitation frequency so that the AN effect can be reduced to a certain extent. However, despite all possible precautions taken at the system design stage, complete elimination of the AN effect is practically impossible. Therefore, even a so-called optimized SHM system might not be able to cope with the requirement needed for small damage detection since the damage-related nonlinearity might still be weaker than the AN-induced nonlinearity.

Meanwhile, existing studies [23-29] show appealing features and great promise of shear horizontal (SH) waves for damage detection applications. Firstly, the fundamental shear horizontal waves (SH0) is non-dispersive in isotropic materials. The wave packet remains undistorted during propagation, thus facilitating the interpretation of the received signals [29-31]. Secondly, the particle motion in SH0 waves is restricted to the in-plane layer [32], thus reducing the coupling with the surrounding medium and possible energy leakage. Moreover, previous investigations based on normal mode expansion (NME)

demonstrate that the power flux from the fundamental SH wave modes to the secondary SH wave modes is zero in a weakly nonlinear plate [23]. In principle, the nonlinearities of the plate and the AN share some similarities, which can be loosely classified as material nonlinearity (MN). However, the main difference between them is that the former is distributed over the plate, while the latter is confined to the PZT actuation area. Therefore, it is interesting to investigate how AN plays out in the context of the 2nd SH waves and whether any benefit can be drawn out of it for potential SHM applications, especially for breathing crack detection. This topic has not been thoroughly discussed in the existing literature.

Motivated by this, a systematic investigation on the detection of breathing cracks in a plate using 2nd SH0 waves is reported in this article. To start with, a theoretical analysis is carried out to understand the underlying mechanisms of the second harmonic generation by the breathing effect of a crack and the material nonlinearity of the bonding layer. By integrating different nonlinear sources, a finite element (FE) model is developed to ascertain the characteristics of the 2nd SH0 waves compared with the conventionally used 2nd Lamb waves. Finally, an experiment is meticulously designed and conducted to demonstrate the superiority of the proposed 2nd-SH0-wave-based crack detection method. For the construction of the SHM system, Magnetostrictive Transducers (MsTs) are used for the generation and reception of SH0 waves. An indenter is used to press on a glass plate specimen with controllable force to create a contact-type crack. By tactically changing the AN through heating the bonding layer, properties of the 2nd-SH0-wave-based system are assessed and compared with the conventional 2nd-Lamb-wave-based system in terms of robustness to AN changes and sensitivity to cracks.

2. Theoretical basis

Consider SH0 waves which are generated by a shear-type transducer and propagate along the x -direction with particles moving along the z -direction, as sketched in Fig. 1. Analyses on the higher harmonic generation by the pure shear deformation in the bonding layer (covering the transducer area) are first qualitatively investigated. The bonding layer is assumed to exhibit weak nonlinear material properties. Then, the mechanism underpinning the interaction between the breathing effect of a contact-type crack with the SH0 waves to generate second harmonic waves is described.

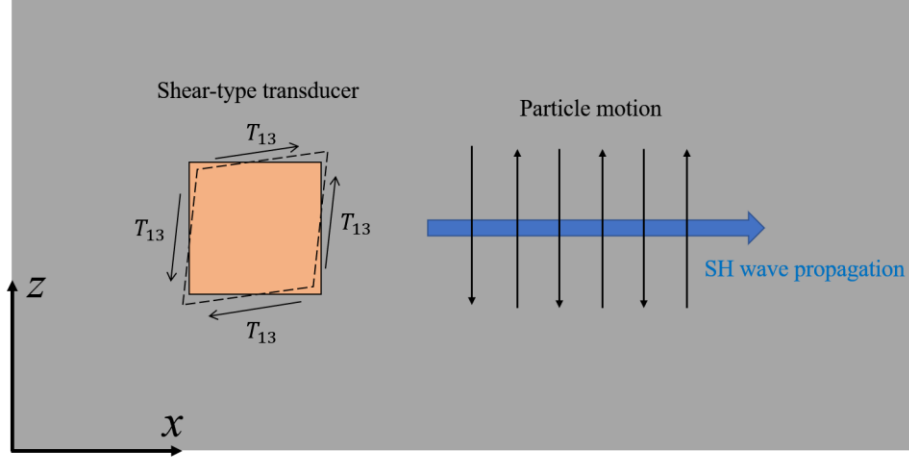


Fig. 1 Schematic of SH wave generation by a face-mounted shear-type transducer and wave propagation in a plate.

2.1 Adhesive nonlinearity for the second harmonic generation

The stress-strain relationship in a weakly nonlinear material can be expressed with the Landau-Lifshitz model [24]. Accordingly, the second Piola-Kirchhoff stress \mathbf{T}^{RR} truncated to the third order writes,

$$\mathbf{T}^{RR} = \lambda \text{tr}[\mathbf{E}] + 2\mu \mathbf{E} + \bar{A} \mathbf{E}^2 + \bar{B} \text{tr}[\mathbf{E}^2] \mathbf{I} + 2\bar{B} \text{tr}[\mathbf{E}] \mathbf{E} + \bar{C} (\text{tr}[\mathbf{E}])^2 \mathbf{I}, \quad (1)$$

where λ and μ are Lamé's constants; \bar{A} , \bar{B} and \bar{C} the Landau third-order elastic

constants (TOECs); $\text{tr}(\)$ represents the trace of a matrix; \mathbf{E} is the Lagrangian strain tensor, in which the geometric nonlinear term can be further omitted under the small deformation assumption. Therefore, the Lagrangian strain E_{ij} retreats to Cauchy's strain S_{ij} while the Cauchy stress T_{ij} is used instead of the second Piola-Kirchhoff stress T_{ij}^{RR} in the following analyses.

A shear-type transducer is surface-bonded on the plate for the generation of SH0 waves, as shown in Fig. 1. The shear stress component T_{13} , which is dominant in the transducer, is transmitted to the plate through a bonding layer, whose shear deformations in the x - z plane should be analyzed. Assuming pure shearing in the x - z plane, the shear stresses and strains in the x - y plane and y - z plane are zero. Meanwhile, the normal stresses are also zero. Then Eq. (1) can be expanded and expressed in terms of individual components as

$$\begin{aligned} 0 = & \lambda(S_{11} + S_{22} + S_{33}) + 2\mu S_{11} + \bar{A}(S_{11}^2 + S_{12}^2 + S_{13}^2) \\ & + \bar{B}(S_{11}^2 + S_{22}^2 + S_{33}^2 + 2S_{13}^2) \\ & + 2\bar{B}(S_{11} + S_{22} + S_{33})S_{11} + \bar{C}(S_{11} + S_{22} + S_{33})^2 \end{aligned} \quad (2)$$

$$\begin{aligned} 0 = & \lambda(S_{11} + S_{22} + S_{33}) + 2\mu S_{22} + \bar{A}(S_{21}^2 + S_{22}^2 + S_{23}^2) \\ & + \bar{B}(S_{11}^2 + S_{22}^2 + S_{33}^2 + 2S_{13}^2) \\ & + 2\bar{B}(S_{11} + S_{22} + S_{33})S_{22} + \bar{C}(S_{11} + S_{22} + S_{33})^2 \end{aligned} \quad (3)$$

$$\begin{aligned} 0 = & \lambda(S_{11} + S_{22} + S_{33}) + 2\mu S_{33} + \bar{A}(S_{31}^2 + S_{32}^2 + S_{33}^2) \\ & + \bar{B}(S_{11}^2 + S_{22}^2 + S_{33}^2 + 2S_{13}^2) \\ & + 2\bar{B}(S_{11} + S_{22} + S_{33})S_{33} + \bar{C}(S_{11} + S_{22} + S_{33})^2 \end{aligned} \quad (4)$$

$$T_{13} = 2\mu S_{13} + 2\bar{B}(S_{11} + S_{22} + S_{33})S_{13} + \bar{A}(S_{11}S_{13} + S_{33}S_{13}) \quad (5)$$

Based on our previous study [21], the normal strains are in the same order of magnitude with S_{13}^2 . Therefore, the normal strains become negligible compared to S_{13} . Any terms in

Eqs. (2) to (5) with the order of magnitude higher than S_{13}^2 can be omitted. The stress-strain relation is further condensed to

$$0 = \lambda(S_{11} + S_{22} + S_{33}) + 2\mu S_{11} + (\bar{A} + 2\bar{B})S_{13}^2 \quad (6)$$

$$0 = \lambda(S_{11} + S_{22} + S_{33}) + 2\mu S_{22} + 2\bar{B}S_{13}^2 \quad (7)$$

$$0 = \lambda(S_{11} + S_{22} + S_{33}) + 2\mu S_{33} + (\bar{A} + 2\bar{B})S_{13}^2 \quad (8)$$

$$T_{13} = 2\mu S_{13} + 2\bar{B}(S_{11} + S_{22} + S_{33})S_{13} + \bar{A}(S_{11}S_{13} + S_{33}S_{13}) \quad (9)$$

By substituting Eqs. (6) to (8) into Eq. (9), the nonlinear shear stress-strain relation writes

$$T_{13} = \mu\gamma_{13} - \left[\frac{12\bar{B}^2 + \bar{A}^2(\lambda/\mu + 2) + 8\bar{A}\bar{B}}{16\mu + 8\lambda} \right] \gamma_{13}^3 \quad (10)$$

where γ_{13} is the commonly-used engineering shear strain, which is related to the shear strain component by $\gamma_{13} = 2S_{13}$. It is worth noting that only the linear and third-harmonic terms of the shear strain appear in Eq. (10), suggesting that no 2nd SH0 waves can be generated in a homogenous material.

2.2 Contact acoustic nonlinearity for second harmonic generations

When micro-scale cracks are physically nucleated with sufficient accumulation of dislocations in a medium, an additional localized contact acoustic nonlinearity (CAN) needs to be addressed. Assuming ultrasonic waves propagate across a crack region, the gap is squeezed under cyclic loading during wave compression and expanded due to wave tension, resulting in the “breathing” behavior. To characterize this process, one of the most popular and straightforward nonlinear crack models is based on bi-linear stiffness [33], also known as stiffness asymmetry [34]. Fig. 2(a) shows the linear shear stress-strain

relation for closed cracks, while Fig. 2(b) shows that no shear stress is transmitted across the surfaces when cracks are open, allowing for a reduced global stiffness [35,36]. The shear stress asymmetry during the crack breathing process yields nonlinear shear stress-strain relationships. Moreover, the roughness between the crack surfaces and the thermal effects may also add to nonlinearities and contribute to the CAN. Friction is a factor for the second harmonic generation, which is also tied with the breathing effect. Specifically, the crack opens and closes subject to the positive and negative shear wave forces for an oblique crack. The normal contact force at the crack interface varies with the crack open/close, resulting in an asymmetrical friction as a result of positive and negative shear forces, thus generating second harmonic waves. For vertical and horizontal cracks, breathing effect disappears and the crack remains closed during the wave propagation. In this case, even with frictions at the crack interface, there will be no asymmetry subjecting to the positive and negative shear forces. Therefore, the second harmonic wave cannot be generated.

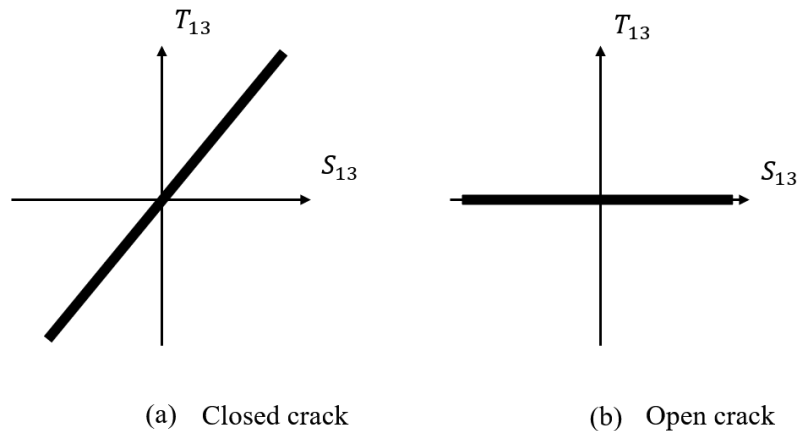


Fig. 2 Shear stress-strain relationships under two crack states [37].

The above brief analyses show that the 2nd SH0 waves can be generated by the primary SH0 wave interaction with a breathing crack but immune to the material nonlinearity of the bonding layer. Upon further confirmation through FE simulations and experimental

investigations, this appealing feature points at an exciting avenue for crack detection, even in the presence of unavoidable nonlinearities from the bonding layers.

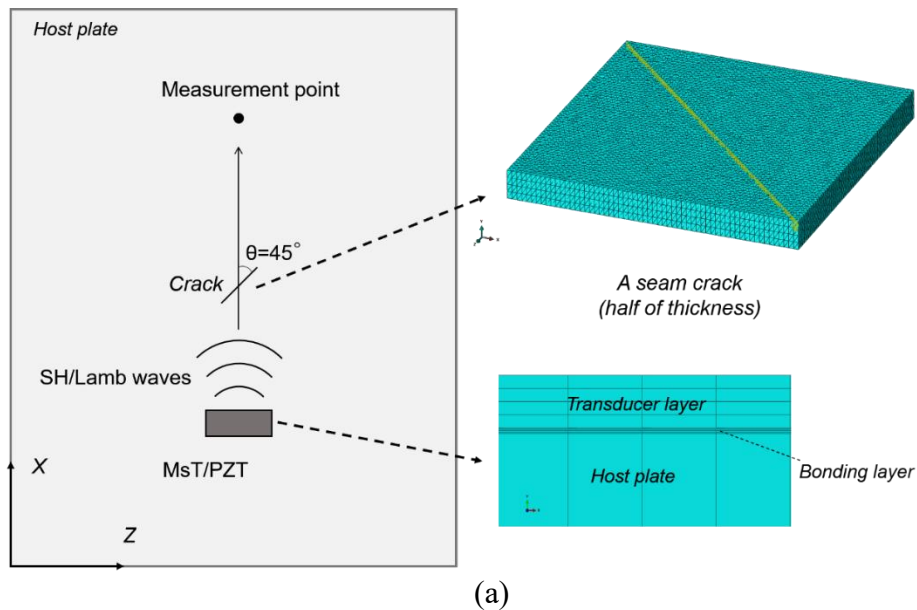
3. Finite element simulation

FE simulations are conducted to investigate the second harmonic waves generated by the CAN of the closed cracks. In addition, the adverse interference of the AN on a typical SHM system is also discussed.

3.1 FE modelling

A schematic diagram of the 3-D FE plate model is shown in Fig. 3(a). The length, width and thickness of the plate are 500, 400 and 3 mm, respectively. The dimension of the plate is determined to strike a balance between the signal complexity resulting from the boundary reflections and the calculation cost. A transducer (an MsT or a PZT) is bonded on the plate through an epoxy adhesive layer of 0.03-mm thick. Instead of using the piezomagnetic or piezoelectric module, an equivalent surface traction is imposed in the simulation for SH or Lamb wave generation in the plate. Based on the theoretical basis, the second harmonic SH wave is immune to non-damaged-related adhesive nonlinearity. In contrast, the second harmonic Lamb wave is inevitably affected by adhesive nonlinearity [22]. Therefore, it is only fair to compare the SH approach with the best scenario of the Lamb wave approach when the adhesive nonlinearity involved in the latter is mitigated as much as practically possible. Meanwhile, the choice of proper excitation frequencies should also ensure that the second harmonic Lamb waves and SH waves can be well measured. The second harmonic Lamb wave system (including the choice of the excitation frequency) is designed

based on our previous work, in which the influence of adhesive nonlinearity is already minimized [22]. The stress σ_{12} on the top surface of the actuator ($30 \times 18 \times 0.3$ mm) mimics the PZT excitation effect, as illustrated in Fig. 3(b). A 5-cycle tone-burst excitation signal, centered at $f_0 = 160$ kHz and modulated by Hann window, is used with a maximum amplitude of 1000 N/m². By contrast, the SH wave system is designed without special consideration on the adhesive nonlinearity. The excitation of the SH waves is simulated by applying the stress σ_{13} on the length side surfaces of the actuator ($30 \times 5 \times 0.1$ mm) to mimic the effect of a magnetostrictive transducer (MsT), as shown in Fig. 3(c). A 12-cycle tone-burst excitation signal, centered at $f_0 = 310$ kHz and modulated by Hann window, is used with the maximum amplitude of 1000 N/m². The smallest wavelength used in the FE simulations, around 5 mm, corresponds to the second harmonic SH0 waves with a 620-kHz central frequency. Therefore, the maximum mesh size (0.25 mm) can ensure around 20 elements per smallest wavelength under consideration.



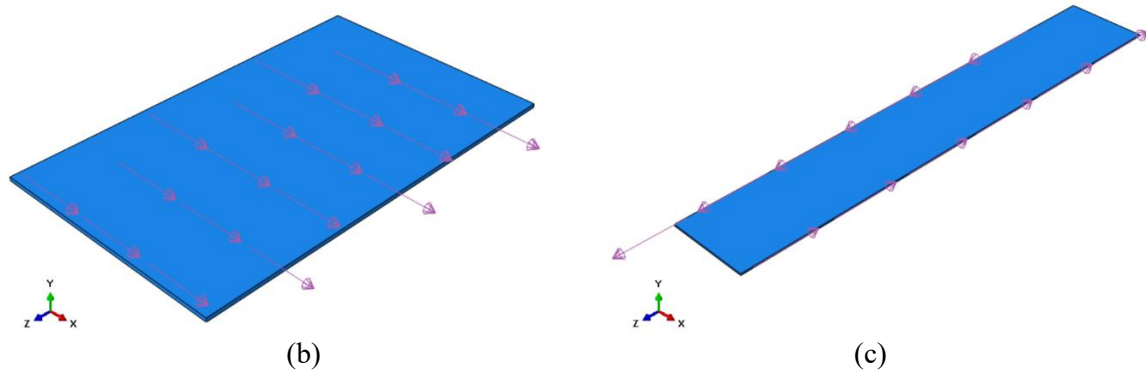


Fig. 3 (a) Schematics of FE simulations with surface traction applied on the (b) top surface of the actuator to mimic the PZT excitation effect; (c) length side surfaces of the actuator to simulate the MsT excitation effect.

Considering the wave propagation along the x -direction, a closed crack is modeled by embedding a half-thickness-through seam, which is sufficiently far from the plate boundaries. The distance between the transducer and the mid-position of the crack is 155 mm. The crack, 35.3-mm long, is 45-degree oblique to the wave propagation direction. To simulate the breathing behavior, the softened contact condition characterized with a linear pressure-overclosure relationship is used for the interaction surfaces, whose slope, k , is set to 7×10^{15} Pa as the contact stiffness [38]. A frictionless condition is considered between the seam interfaces. The signal reception point is 110 mm away from the crack to capture the forward-propagation primary waves generated by the actuator and the second harmonics generated by the primary waves after interacting with the crack. The AN is also included in the model by embedding the Landau-Lifshitz stress-strain relation in Eq. (3) to Abaqus[®]/EXPLICIT through user subroutine VUMAT. It should be noted that the second harmonic responses at a fixed position before and after the crack is generated. Therefore, the cumulative effect of nonlinear waves generated by different nonlinear sources is not the major concern from the detection perspective. Having said that, it has been well demonstrated in our previous work [39] that the second harmonic Lamb wave generated

by adhesive nonlinearity is not cumulative due to its localized nature. The same applied to the rather localized cracks which are considered in this work.

3.2 FE results and discussions

The material properties of each component used in the FE models are tabulated in Table 1. Linear mechanical properties of the transducers and the plate are considered, while the bonding layer has nonlinear elastic properties. The TOECs of the adhesive are taken from Ref. [40]. The second harmonic components in the FE results are extracted using the superposition method [21] by superposing two response signals due to two excitations with opposite phases. The method, as demonstrated before, allows eliminating the linear and odd harmonic components.

Table 1. Material parameters used in the FE models

Host plate					
Length	Width	Thickness	ρ	E	ν
500 mm	400 mm	3 mm	2500 GPa	88 GPa	0.215
PZT					
Length	Width	Thickness	ρ	E	ν
30 mm	18 mm	0.3 mm	7500 kg/m ³	62 GPa	0.32
MsT					
Length	Width	Thickness	ρ	E	ν
30 mm	5 mm	0.1 mm	7800 kg/m ³	200 GPa	0.269
Bonding Layer					
Thickness	E	ν	A	B	C
0.03 mm	1.31 GPa	0.4	-20.9 GPa	-8.3 GPa	-6.1 GPa

An actuator (an MsT or a PZT) is bonded on the plate to generate either SH waves or Lamb waves. Generated waves propagate through the crack to trigger the “breathing” behavior to generate the CAN. The SH wave case is first considered. The interaction between the probing SH waves and the contact-type crack is illustrated in Fig. 4. From the cross-sectional view on the x - z plane, cutting through the crack, it can be seen that the SH-

wave-induced particle displacements along the z -direction are continuously transmitted through the crack when it is closed while being interrupted when opened.

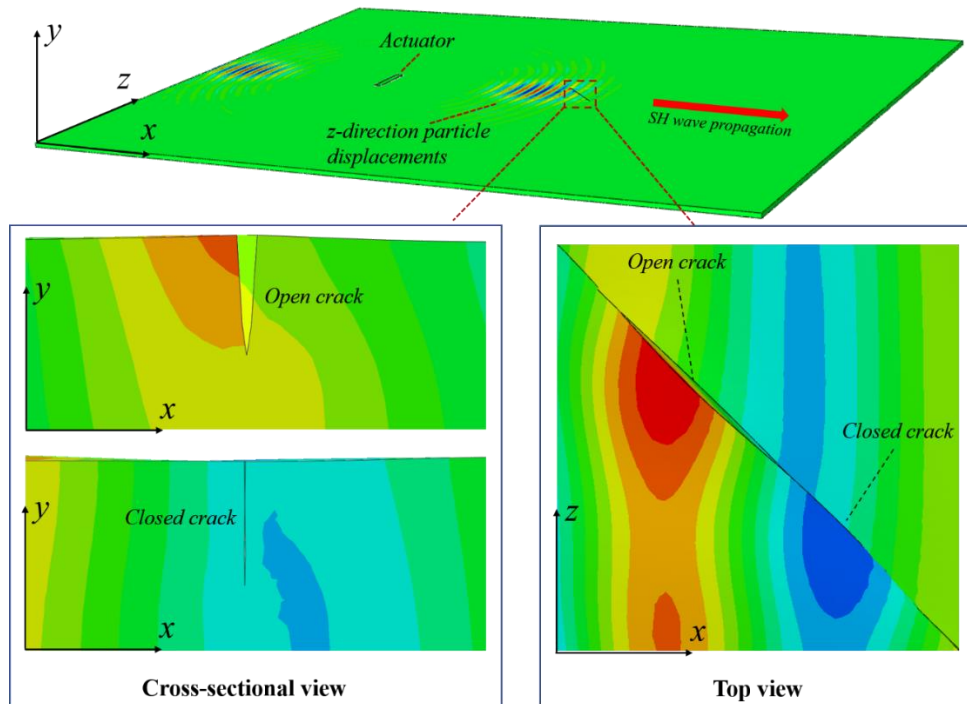


Fig. 4 Snapshots of SH waves traversing a half-thickness-through closed crack with CAN in modelling

3.2.1 Comparisons between undamaged case and cracked case

The linear and nonlinear time-domain responses of SH waves, in terms of the z -direction particle displacements captured at the reception point, are investigated by considering the AN. As illustrated in Fig. 5(a), the crack produces negligible changes in the amplitude of the overall primary SH₀ mode responses as expected. Using the superposition method, the second harmonics of the undamaged and the cracked cases are extracted and compared in Fig. 5(b). No 2nd SH₀ response can be seen in the undamaged plate even with the presence of the AN. This confirms the previous analysis in that the material nonlinearity in a homogenous material does not introduce 2nd harmonic waves into the SH wave field. Adding the breathing crack into the plate, a noticeable change is observed. The new wave

packet appears with a similar group velocity as the primary SH0 mode (seen in Fig. 5(a)) but with a shorter wavelength, corresponding to the 2nd SH0 mode generated by the CAN.

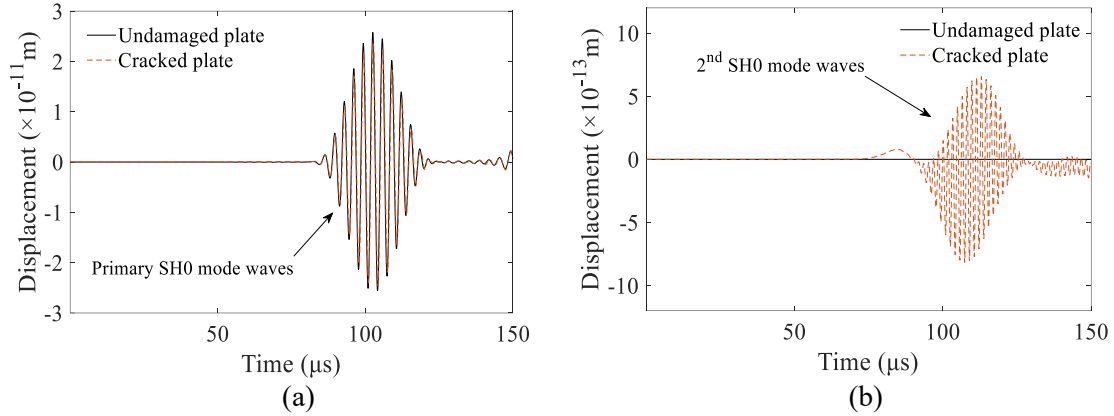


Fig. 5 Numerically simulated responses (z -direction displacement) corresponding to the undamaged-plate and cracked-plate cases; (a) primary SH waves; and (b) 2nd SH waves.

Following the same procedure, the linear and nonlinear Lamb wave responses are compared, before and after introducing the crack. The time-domain x -direction nodal displacements are captured at the same reception point as in the SH wave case. Based on the dispersion curves of Lamb waves, only S0 and A0 modes exist in the frequency range under consideration. The S0 mode features a higher group velocity than the A0 mode, which helps distinguish two clear wave packets, as shown in Fig. 6(a). The captured primary S0 waves show almost imperceptible changes in amplitude and phase, demonstrating the deficiency of the linear wave components for closed crack detection. Using the aforementioned superposition method again, the corresponding second harmonic Lamb wave responses are extracted and compared in Fig. 6(b). It can be seen that the amplitude of the 2nd S0 mode experiences a significant increase with the introduction of the breathing crack. Nevertheless, the FE results also indicate that there are inevitable 2nd Lamb waves in the system before introducing the crack.

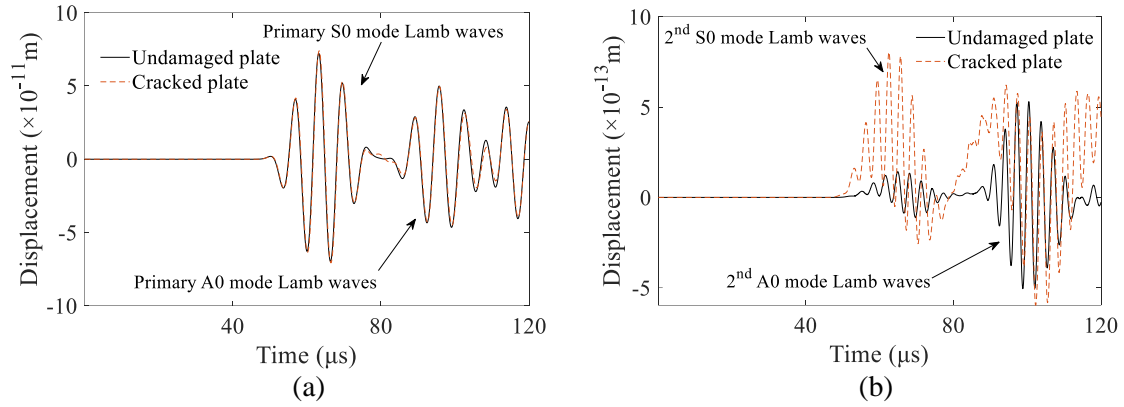


Fig. 6 Numerical simulated responses (x -direction displacement) corresponding to the undamaged-plate and cracked-plate cases as (a) primary Lamb waves; and (b) 2nd Lamb waves.

3.2.2 Variations of 2nd SH waves along with crack directions

With the developed FE models, the CAN-induced 2nd SH0 waves are examined for different crack directions. The angle between the crack extension direction and the wave propagation direction is varied as 0° , 22.5° , 45° , 67.5° , and 90° , as shown in Fig. 7. To accurately quantify the 2nd SH waves, complex Morlet transform is applied. The peak values of the corresponding modulus of the wavelet coefficient at 320 kHz in each case are extracted and compared directly. The results first show that no 2nd SH wave is generated when the crack is parallel or perpendicular to the wave propagation direction. The physical interpretation is that the particles on both sides of the crack have the same vibration amplitude and direction. As a result, no tensile-compression asymmetry occurs, thus leading to no breathing phenomenon. This is why no 2nd SH wave is generated when approaching these two specific angles. The results demonstrate the reduced detectability of the 2nd SH waves when approaching these two specific angles. By contrast, the maximum detection sensitivity can be obtained for a 45-degree oblique crack. These results provide useful references for the experimental design in the subsequent sections.

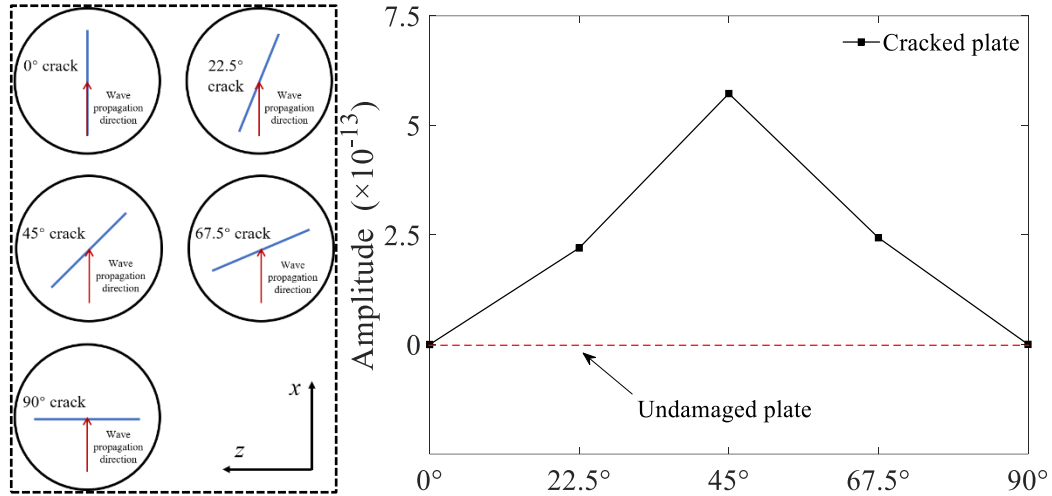


Fig. 7 Variations of 2nd SH amplitudes along with the crack directions.

To sum up, FE studies confirm that both the 2nd SH0 mode and 2nd S0 mode waves have higher sensitivities to the closed crack than their linear counterparts, which is consistent with the theoretical analyses. When comparing the undamaged-plate case with the crack-plate cases, the primary linear responses in Fig. 5(a) and Fig. 6(a) in the manuscript show almost imperceptible changes in terms of both amplitude and phase. These results demonstrate the deficiency of the linear wave components for closed crack detection. By contrast, both the 2nd S0 waves and 2nd SH0 waves undergo significant changes, clearly indicating the presence of the closed crack. When considering the AN in the FE models, the material-nonlinearity-induced 2nd S0 mode waves are generated, which may potentially disrupt the effective detection of the CAN. By contrast, no 2nd SH wave is generated by the AN, in agreement with theoretical analyses. The measured 2nd SH0 mode waves can only be attributed to the crack-induced CAN. Experiments in the subsequent sections will further verify these findings.

4. Experimental validations

Experiments are carried out to validate the proposed 2nd-SH0-wave-based damage detection method by following a two-step procedure. First, the capability of the 2nd SH waves for closed crack detection is validated. Then, their expected immunity to the homogeneously material nonlinearities is experimentally demonstrated.

4.1 Experimental set-up

Considering the difficulty in producing controllable cracks using conventional cyclic loading in metals, a Soda-lime-silica glass panel specimen was used in experiments. The panel has very close properties to the one used in the above FE analyses. An indenter was used to hit the panel and create a crack in its central region. The load was gradually increased until the appearance of a crack of 40-mm long, as shown in Fig. 8. After the hitting, the crack remained closed without any material removal, thus ensuring crack opening and closing when guided waves pass through, typical of the realistic “breathing” behavior of a crack.

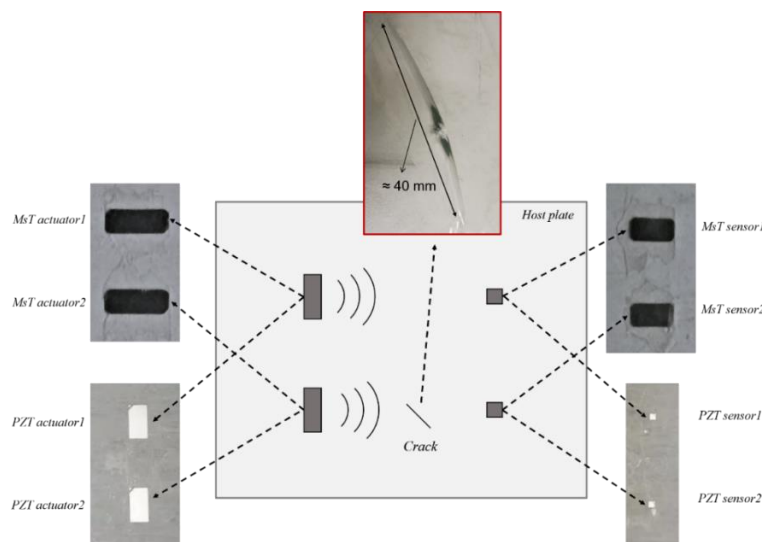


Fig. 8 Sketch of the experimental set-up.

MsTs and PZTs were used for the generation and reception of the SH waves and Lamb waves, respectively. PZTs were first installed on the panel for Lamb waves before they were removed and replaced by MsTs at the same position for SH waves. This allows for a direct comparison of the two systems using the same panel in a consistent manner. The transducers were bonded onto the panel by applying the same pressure force to ensure consistency in the bonding conditions as much as practically possible. In both Lamb and SH wave systems, two wave propagation paths, connecting the wave emission and reception points, are considered: one as the undamaged path; and the other one as the cracked path passing through the breathing crack. In the SH wave system, the MsT actuator has a coil with fold number $N_f = 5$ and a periodicity distance $D = 10.3$ mm, as sketched in Fig. 9. This configuration was specifically designed for the effective generation of 310-kHz SH₀ waves in the panel. As for the sensor, a 5-fold coil with $D = 5.2$ mm was used to measure 2nd SH₀ waves. This sensor is very sensitive to the SH waves at around 620 kHz but a lot less at the fundamental SH waves (at about 310 kHz). Details about the MsT component design and rationales can be found in Refs. [41,42]. The RITEC RAM-5000-SNAP system was used to generate a 12-cycle tone-burst pulse with a central frequency of 310 kHz for the excitation of SH waves.

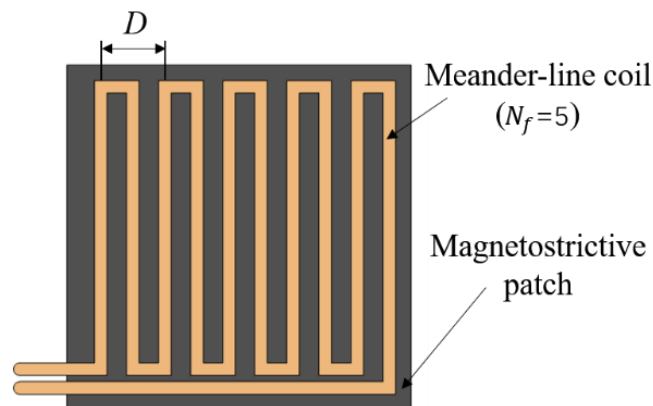


Fig. 9 Sketch of the meander-line coil used in the MsT-activated SHM system.

As to the PZT-activated Lamb wave system, the configuration of the actuator and the excitation frequency was carefully designed to minimize the influence of the non-damage-related AN with the method proposed in our previous work [22]. More specifically, an 18-mm wide PZT actuator was used for the excitation of the primary S0 mode Lamb waves at 160 kHz. The width of the PZT sensor was 5 mm. Measurement was made by the National Instrument (NI) system, with details described in our previous work [21]. In each test, 200 signals were averaged to minimize the influence of the measurement noise. In addition, the process was repeated five times further to calculate the variation range of the measured results.

4.2 Evaluation of the crack detection capabilities

Results from the PZT-activated Lamb wave system are shown in Figs. 10(a) and 10(b), including the measured linear and nonlinear signals obtained from the undamaged path and the cracked path, respectively. The linear responses plotted in Fig. 10(a) show that the excitation levels of the S0 mode waves in the two propagation paths are almost the same, demonstrating that the transducers were well installed to guarantee the comparability of results from the two paths. Therewith, further extracting the second harmonic components using the superposition method allows the comparison between the two paths, as shown in Fig. 10(b). For the undamaged path, the 2nd S0 mode waves are attributed to the AN, despite all the system design precautions (as discussed before). As to the cracked path, the 2nd S0 mode response shows a larger amplitude. Compared with the undamaged path, the increased energy level confirms the generation of the second harmonics by the crack.

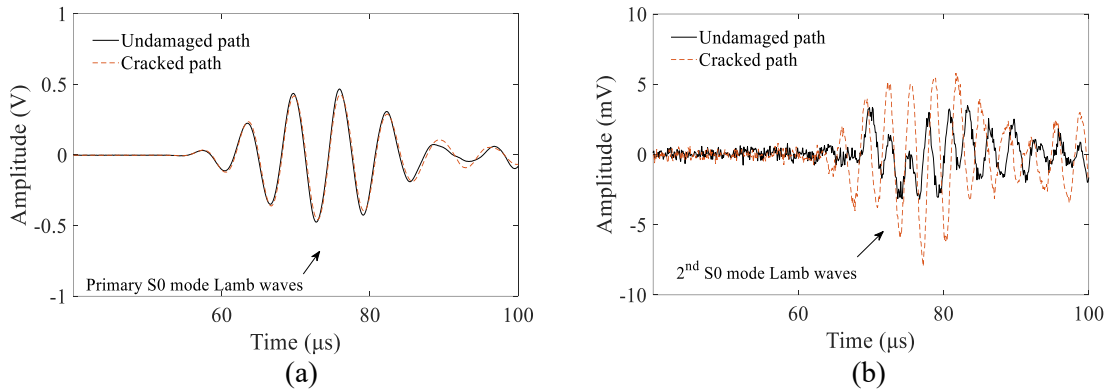


Fig. 10 Comparison of experimental results obtained from the undamaged path and the cracked path: (a) S0-mode linear time-domain responses; and (b) second order components of (a).

Following the same procedure, results from the MsT-activated SH system are presented in Figs.11(a) and 11(b). As one may expect, the linear SH0 responses show no apparent difference between the two paths, as illustrated in Fig.11(a). For the second harmonic responses shown in Fig. 11(b), weak second harmonics in the undamaged path are observed, which may be attributed to the nonlinearity of the instruments and the unavoidable weak Lamb waves in the system. Nevertheless, a single prominent wave packet of the 2nd SH0 mode appears in the cracked path, demonstrating the higher sensitivity of the 2nd SH0 waves for breathing cracks.

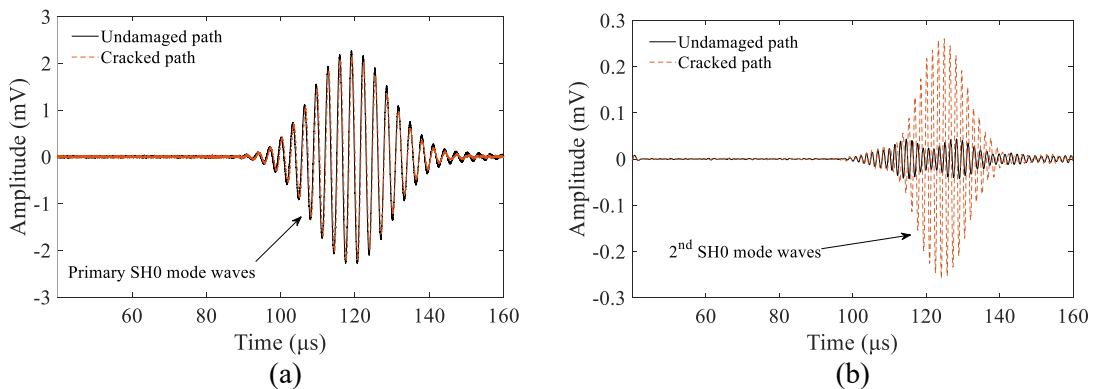


Fig. 11 Comparison of experimental results obtained from the undamaged path and cracked path: (a) SH0-mode linear time-domain responses; and (b) second order components of (a).

The above experimental results first confirm that both the 2nd Lamb waves and the 2nd SH waves can be used to detect the closed crack. However, even without any crack, the

inevitable nonlinear source causes the 2nd Lamb waves, which interfere with the crack-induced 2nd Lamb wave responses. By contrast, the non-damage-related 2nd SH waves show a relatively low energy level. After passing through the crack, the significantly increasing trend in the 2nd SH waves testifies their higher capability for crack detection than the 2nd Lamb waves.

4.3 Influence of the AN on CAN-induced second harmonics

To further demonstrate the superiority of the 2nd SH₀ waves for crack detection, the level of the AN in both systems was tactically changed through a specially designed thermal treatment. The applied thermal treatment was expected to change the material nonlinear properties of the bonding layer, which is epoxy in this case. Previous studies [21] show that the effect of the AN in the actuating part is more significant than that in the sensing part. Therefore, the thermal treatment was applied only to the bonding layer under the actuator. More specifically, a small region of 100×100 mm covering the actuation area was heated to around 70 °C for 2 hours. After heating, measurements were conducted again for both Lamb wave and SH wave systems. It is worth noting that the heating temperature is no more than 70 °C, which is shown to create no noticeable changes in the operation of the transducers (MsTs or PZTs). Therefore, only tiny changes occur in the primary waves. Then, the major concern is about the heating effect on the bonding layer, in which the AN is supposed to be significantly changed.

For the PZT-activated system, after heating, the amplitudes of the time-domain signals of the second harmonics along both the undamaged and cracked paths show a noticeable increase, as illustrated in Figs. 12(a) and 12(c). To quantify the changes, a complex Morlet

transform is used, yielding the corresponding modulus of the wavelet coefficient at 320 kHz, as shown in Figs. 12(b) and 12(d). The observed changes suggest that the 2nd-S₀-wave-based crack detection method is vulnerable to non-damage-related nonlinear sources, exemplified by the AN in this particular test. Such influence may overwhelm the useful damage-related information, thus causing erroneous evaluation of the damage severity.

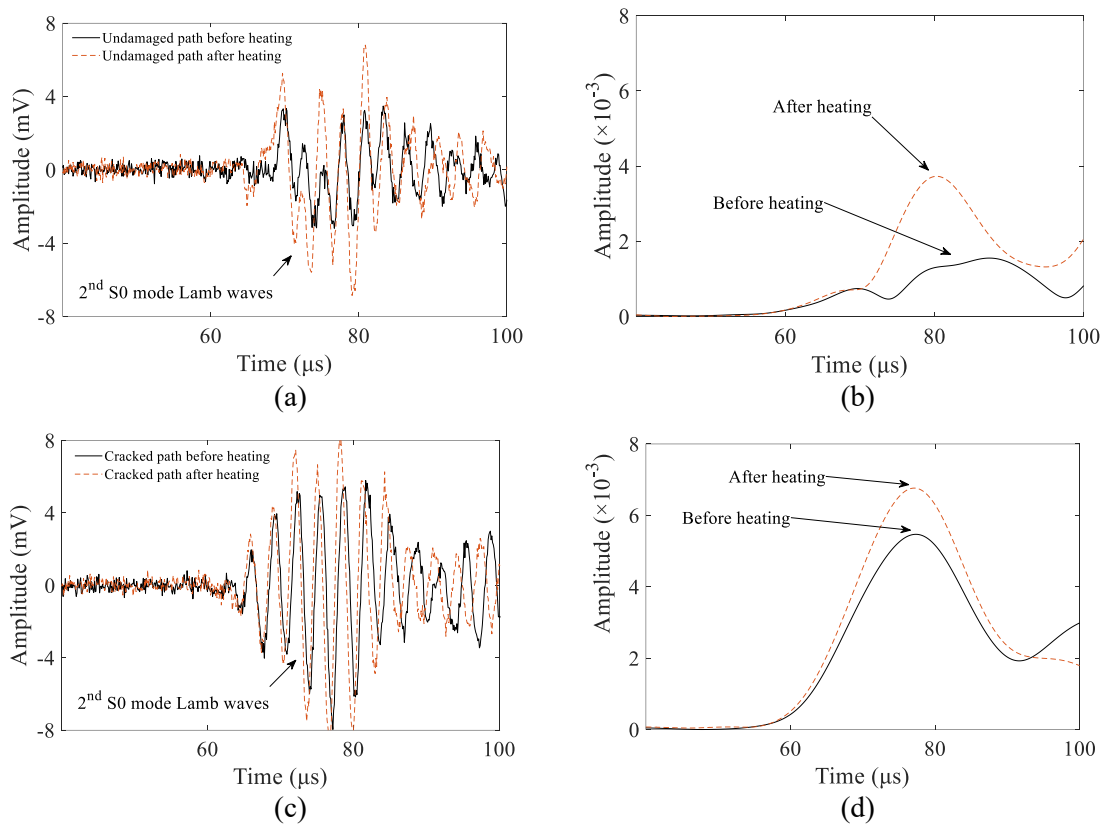


Fig. 12 PZT-activated SHM system results before and after heating treatment for bonding layer: (a) second harmonic time-domain responses in the undamaged path; (b) the modulus of the wavelet coefficient at 320 kHz of (a); (c) second harmonic time-domain responses in the cracked path; (d) the modulus of the wavelet coefficient at 320 kHz of (c).

For comparison, the same thermal treatment was applied to the MsT-activated SH wave system. Comparisons in terms of the measured 2nd SH₀ signals before and after the heating are shown in Figs. 13(a) to 13(d). The weak 2nd harmonics in the undamaged path undergo a certain level of change because weak Lamb waves can still be generated and received by

the MsT activated system. As for the cracked path, time-domain signals show no significant differences (3%) to the thermal-induced AN property changes, as confirmed by corresponding complex Morlet transform results (Fig. 13(d)). Again, the observed slight differences in the amplitude are attributed to the change of the weak Lamb waves. Despite this, the observed energy level changes in the 2nd SH0 signals are much less than the 2nd Lamb waves (30 %). This confirms the theoretically and numerically predicted immunity of the 2nd SH0 signals to the AN.

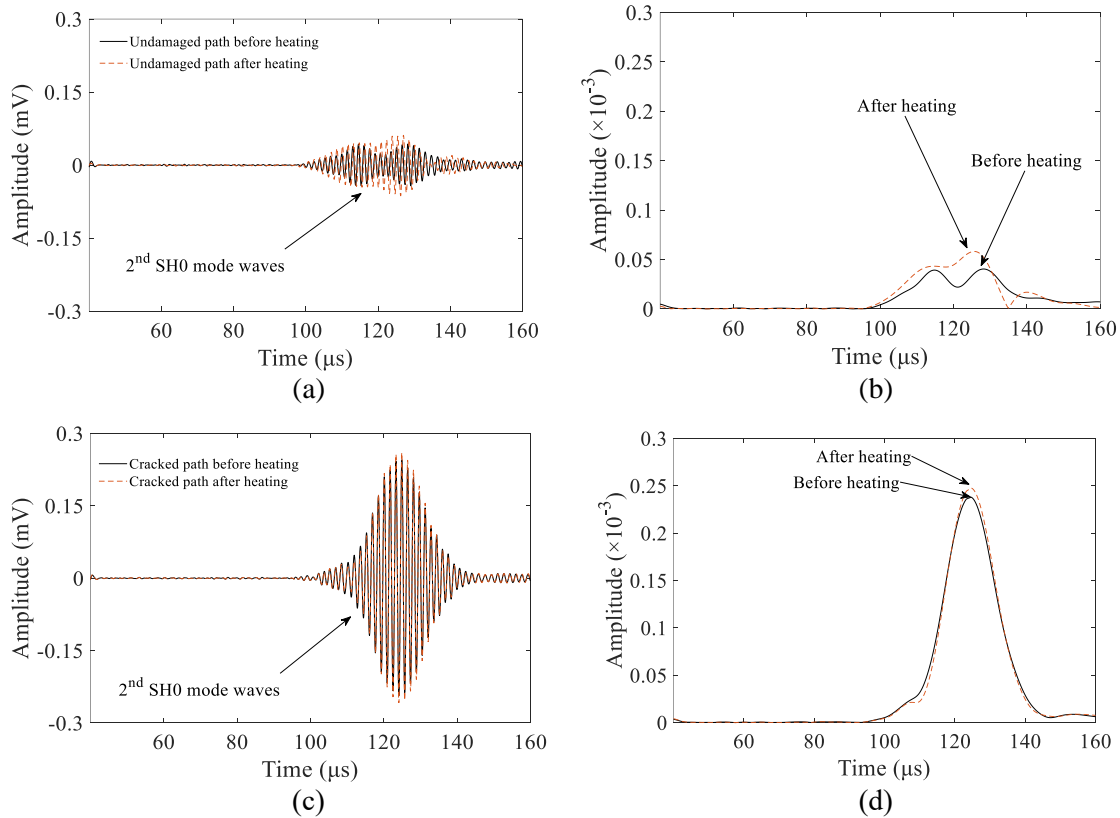
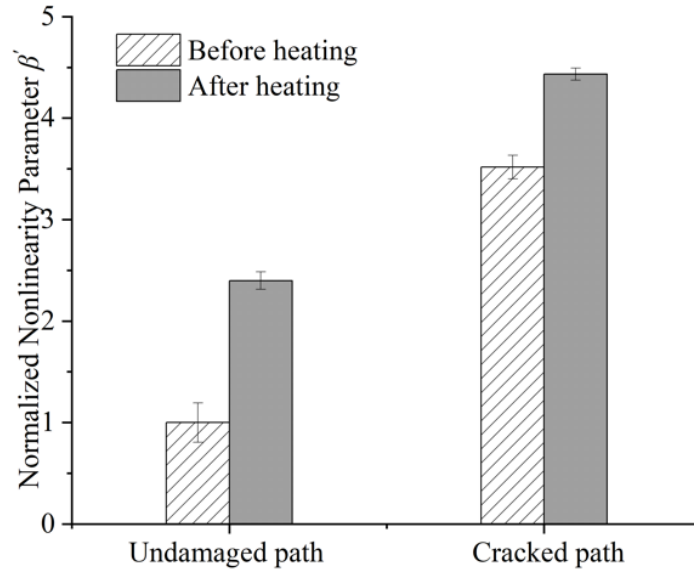


Fig. 13 MsT-activated SHM system results before and after heating treatment for bonding layer: (a) second harmonic time-domain responses in the undamaged path; (b) the modulus of the wavelet coefficient at 620 kHz of (a); (c) second harmonic time-domain responses in the cracked path; (d) the modulus of the wavelet coefficient at 620 kHz of (c).

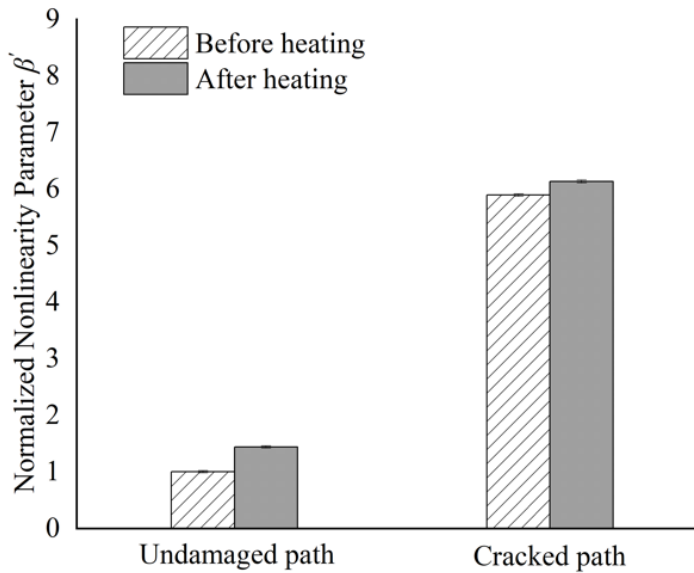
To quantify the degree of changes, the conventionally used relative acoustic nonlinearity parameter β' is adopted, defined as

$$\beta' = \frac{A_2}{A_1^2}, \quad (11)$$

where A_1 is the magnitude of the primary waves while A_2 that of the second harmonic waves. As illustrated before, the measurement process was repeated five times to obtain the corresponding time-domain responses. Each process is based on averaged value from 200 signals. The magnitudes involved in the calculation are obtained by extracting the peak value of the modulus of wavelet coefficients. β' is calculated for each of the five repetitive cases above and normalized to the result of the undamaged case (Fig. 10(b) for the 2nd Lamb waves and Fig. 11(b) for 2nd SH waves). Consequently, the corresponding mean results alongside error bars are plotted in Figs. 14(a) and 14(b). Results before heating show dramatic changes in both the 2nd Lamb waves (245.9% increase) and the 2nd SH waves (516.3% increase), mainly attributed to the CAN-induced second harmonics. After heating the bonding layer in the actuation part, an increase (30%) can be observed in the 2nd Lamb waves. This significant change in the nonlinear responses can only be attributed to the AN changes as a result of the thermal treatment. By contrast, results indicate only a very slight increase (3%) in the 2nd SH waves after the same thermal treatment procedure. Again, the 2nd SH waves show higher robustness to the variation of the AN.



(a)



(b)

Fig. 14 Summaries of the normalized relative acoustic nonlinearity parameter β' from each case with error bars in: (a) PZT-activated SHM system; (b) MsT-activated SHM system.

To sum up, experiments establish that the “breathing” crack detection method based on 2nd SH waves is more effective and reliable than the one using the 2nd Lamb waves. This originates from the increased robustness of the 2nd SH waves against AN and their appreciable sensitivity to CAN. Both features are beneficial to crack detection.

5. Conclusions

The second harmonic SH0 wave generation and its interaction with a closed crack and adhesive layers in an autonomous SHM system are investigated in this paper. A theoretical analysis is first conducted to explain the second harmonic generation due to the CAN and AN. Based on this, FE analyses are performed to validate and confirm the theoretical findings on the nonlinear material properties of the bonding layer. Introducing a seam crack into the 3-D FE model, S0 mode Lamb wave and SH0 mode wave interactions with the CAN are scrutinized. Upon tactically designing the system configuration and the thermal aging treatment, experiments are conducted to demonstrate the high sensitivity of the 2nd SH0 waves to the “breathing” crack and their increased immunity to the AN, checked against their 2nd S0 mode wave counterparts.

Both theoretical analyses and numerical studies demonstrate that, in principle, the AN of the bonding layers under SH wave actuators cannot generate the 2nd SH waves in a weakly nonlinear plate. Although this cannot be perfectly realized due to the unavoidable existence of weak Lamb wave components in a practical measurement system, the phenomenon is qualitatively confirmed by experiments through cross-checking with their 2nd S0 mode wave counterparts. While the 2nd S0 mode waves are vulnerable to the variations of the material nonlinearities in the system, the 2nd SH0 waves offer much-enhanced immunity while preserving its appreciable sensitivity to the crack-induced CAN. Given the same level of AN variation and a breathing crack, it has been experimentally shown that the 2nd SH0 waves present appealing properties for closed crack detection, as evidenced by a significant and AN-proof increase in the relative acoustic nonlinearity parameter β' .

The glass specimen is used in the experiments as a proof-of-concept of the proposed method because it is easier to create a controllable contact-type crack without material loss in a glass than in metals. The proposed method will certainly be extended to metallic and other engineering structures, which definitely requires further miscellaneous examinations as future work. In addition, the challenges in SH wave generation and reception methods are well known. New technological advances are needed to boost the SH-wave-based SHM techniques for practical applications.

Acknowledgments

The project was supported by grants from the Research Grants Council of Hong Kong Special Administrative Region (PolyU 152070/16E), the National Natural Science Foundations of China through SHENG project (Polish-Chinese Funding Initiative, 51961135302), and the Innovation and Technology Commission of the HKSAR Government to the Hong Kong Branch of National Rail Transit Electrification and Automation Engineering Technology Research Center. The authors would like to acknowledge Prof. Wieslaw J. Staszewski from AGH University of Science and Technology for the preparation of the cracked glass specimen.

References

- [1] Jhang, K. Y. Nonlinear ultrasonic techniques for nondestructive assessment of micro damage in material: A review (vol 10, pg 123, 2009). *Int J Precis Eng Man* **18**, 139-139, (2009).
- [2] Radecki, R., Su, Z. Q., Cheng, L., Packo, P. & Staszewski, W. J. Modelling nonlinearity of guided ultrasonic waves in fatigued materials using a nonlinear local interaction simulation approach and a spring model. *Ultrasonics* **84**, 272-289, (2018).
- [3] Fierro, G. P. M., Ciampa, F., Ginzburg, D., Onder, E. & Meo, M. Nonlinear ultrasound modelling and validation of fatigue damage. *J Sound Vib* **343**, 121-130, (2015).
- [4] Deng, M. X. Analysis of second-harmonic generation of Lamb modes using a modal analysis approach. *J Appl Phys* **94**, 4152-4159, (2003).
- [5] Bermes, C., Kim, J. Y., Qu, J. M. & Jacobs, L. J. Nonlinear Lamb waves for the detection of material nonlinearity. *Mech Syst Signal Pr* **22**, 638-646, (2008).
- [6] Dutta, D., Sohn, H., Harries, K. A. & Rizzo, P. A Nonlinear Acoustic Technique for Crack Detection in Metallic Structures. (vol 8, pg 251, 2009). *Struct Health Monit* **8**, 573-573, (2009).
- [7] Zhou, C., Hong, M., Su, Z. Q., Wang, Q. & Cheng, L. Evaluation of fatigue cracks using nonlinearities of acousto-ultrasonic waves acquired by an active sensor network. *Smart Mater Struct* **22**, (2013).
- [8] Pruell, C., Kim, J. Y., Qu, J. & Jacobs, L. J. A nonlinear-guided wave technique for evaluating plasticity-driven material damage in a metal plate. *Ndt&E Int* **42**, 199-203, (2009).
- [9] Yang, Y., Ng, C. T., Kotousov, A., Sohn, H. & Lim, H. J. Second harmonic generation at fatigue cracks by low-frequency Lamb waves: Experimental and numerical studies. *Mech Syst Signal Pr* **99**, 760-773, (2018).
- [10] An, Y. K. & Sohn, H. Visualization of non-propagating Lamb wave modes for fatigue crack evaluation. *J Appl Phys* **117**, (2015).
- [11] Khassestarash, A. & Hassennejad, R. Energy dissipation caused by fatigue crack in beam-like cracked structures. *J Sound Vib* **363**, 247-257, (2016).
- [12] Scarselli, G., Ciampa, F., Ginzburg, D. & Meo, M. Non-Destructive Testing techniques based on nonlinear methods for assessment of debonding in single lap joints. *Structural Health Monitoring and Inspection of Advanced Materials, Aerospace, and Civil Infrastructure 2015* **9437**, (2015).
- [13] Shui, G. S., Wang, Y. S., Huang, P. & Qu, J. M. Nonlinear ultrasonic evaluation of the fatigue damage of adhesive joints. *Ndt&E Int* **70**, 9-15, (2015).
- [14] Broda, D., Pieczonka, L., Hiwarkar, V., Staszewski, W. J. & Silberschmidt, V. V. Generation of higher harmonics in longitudinal vibration of beams with breathing cracks. *J Sound Vib* **381**, 206-219, (2016).
- [15] Guha, A. & Bijudas, C. R. Higher and Sub-harmonic Lamb wave mode generation due to debond-induced contact nonlinearity. *Health Monitoring of Structural and Biological Systems 2016* **9805**, (2016).
- [16] Destrade, M. & Ogden, R. W. On the third- and fourth-order constants of incompressible isotropic elasticity. *J Acoust Soc Am* **128**, 3334-3343, (2010).
- [17] Lissenden, C. J., Liu, Y., Choi, G. W. & Yao, X. Effect of Localized Microstructure

- Evolution on Higher Harmonic Generation of Guided Waves. *J Nondestruct Eval* **33**, 178-186, (2014).
- [18] Choi, G., Liu, Y., Yao, X. C. & Lissenden, C. J. Effect of Localized Microstructural Evolution on Higher Harmonic Generation of Guided Wave Modes. *41st Annual Review of Progress in Quantitative Nondestructive Evaluation, Vol 34* **1650**, 1592-1598, (2015).
- [19] Chillara, V. K. & Lissenden, C. J. Nonlinear guided waves in plates: A numerical perspective. *Ultrasonics* **54**, 1553-1558, (2014).
- [20] Chillara, V. K. & Lissenden, C. J. Nonlinear Guided Waves in Plates Undergoing Localized Microstructural Changes. *41st Annual Review of Progress in Quantitative Nondestructive Evaluation, Vol 34* **1650**, 1561-1569, (2015).
- [21] Shan, S. B., Cheng, L. & Li, P. Adhesive nonlinearity in Lamb-wave-based structural health monitoring systems. *Smart Mater Struct* **26**, (2017).
- [22] Shan, S. B., Cheng, L. & Wen, F. Z. Design of nonlinear-Lamb-wave-based structural health monitoring systems with mitigated adhesive nonlinearity. *Smart Mater Struct* **27**, (2018).
- [23] Liu, Y., Chillara, V. K. & Lissenden, C. J. On selection of primary modes for generation of strong internally resonant second harmonics in plate. *J Sound Vib* **332**, 4517-4528, (2013).
- [24] Liu, Y., Chillara, V. K., Lissenden, C. J. & Rose, J. L. Third harmonic shear horizontal and Rayleigh Lamb waves in weakly nonlinear plates. *J Appl Phys* **114**, (2013).
- [25] Shan, S. & Cheng, L. Mixed third harmonic shear horizontal wave generation: interaction between primary shear horizontal wave and second harmonic Lamb wave. *Smart Mater Struct* **28**, 085042, (2019).
- [26] Wen, F., Shan, S. & Cheng, L. Third harmonic shear horizontal waves for material degradation monitoring. *Structural Health Monitoring*, 1475921720936983, (2020).
- [27] Giurgiutiu, V. *Structural health monitoring: with piezoelectric wafer active sensors*. (Elsevier, 2007).
- [28] Seung, H. M., Kim, H. W. & Kim, Y. Y. Development of an omni-directional shear-horizontal wave magnetostrictive patch transducer for plates. *Ultrasonics* **53**, 1304-1308, (2013).
- [29] Kamal, A. & Giurgiutiu, V. Shear horizontal wave excitation and reception with shear horizontal piezoelectric wafer active sensor (SH-PWAS). *Smart Mater Struct* **23**, (2014).
- [30] Zhou, W. S., Li, H. & Yuan, F. G. Fundamental understanding of wave generation and reception using d(36) type piezoelectric transducers. *Ultrasonics* **57**, 135-143, (2015).
- [31] Li, P., Shan, S. B., Wen, F. Z. & Cheng, L. A fully-coupled dynamic model for the fundamental shear horizontal wave generation in a PZT activated SHM system. *Mech Syst Signal Pr* **116**, 916-932, (2019).
- [32] Belanger, P. & Boivin, G. Development of a low frequency omnidirectional piezoelectric shear horizontal wave transducer. *Smart Mater Struct* **25**, (2016).
- [33] Worden, K. *Nonlinearity in structural dynamics: detection, identification and modelling*. (CRC Press, 2019).

- [34] Solodov, I. Y., Krohn, N. & Busse, G. CAN: an example of nonclassical acoustic nonlinearity in solids. *Ultrasonics* **40**, 621-625, (2002).
- [35] Friswell, M. I. & Penny, J. E. Crack modeling for structural health monitoring. *Structural health monitoring* **1**, 139-148, (2002).
- [36] Gudmundson, P. The dynamic behaviour of slender structures with cross-sectional cracks. *Journal of the Mechanics and Physics of Solids* **31**, 329-345, (1983).
- [37] Kawashima, K., Omote, R., Ito, T., Fujita, H. & Shima, T. Nonlinear acoustic response through minute surface cracks: FEM simulation and experimentation. *Ultrasonics* **40**, 611-615, (2002).
- [38] Shen, Y. & Giurgiutiu, V. Predictive modeling of nonlinear wave propagation for structural health monitoring with piezoelectric wafer active sensors. *Journal of Intelligent Material Systems and Structures* **25**, 506-520, (2014).
- [39] Shan, S., Cheng, L. & Wen, F. Characterization of nonplanar second harmonic Lamb waves with a refined nonlinear parameter. *Journal of Nondestructive Evaluation, Diagnostics and Prognostics of Engineering Systems* **1**, (2018).
- [40] Landau, L. D., Lifshits, E. M., Kosevich, A. M. & Pitaevskiĭ, L. P. *Theory of elasticity*. 3rd English edn, (Pergamon Press, 1986).
- [41] Wen, F., Shan, S., Radecki, R., Staszewski, W. J. & Cheng, L. Shear-lag modelling of surface-bonded magnetostrictive transducers for shear horizontal wave generation in a non-ferromagnetic plate. *Smart Mater Struct* **30**, 035026, (2021).
- [42] Cho, H., Hasanian, M., Shan, S. & Lissenden, C. J. Nonlinear guided wave technique for localized damage detection in plates with surface-bonded sensors to receive Lamb waves generated by shear-horizontal wave mixing. *Ndt&E Int* **102**, 35-46, (2019).